AGU PUBLICATIONS

Global Biogeochemical Cycles

RESEARCH ARTICLE
10.1002/2015GB005186

Key Points:
- Biogenic Si burial south of 40°S is 2.3 ± 1.0 Tmol per yr
- Maximum opal burial decreases with increasing number of ice-covered days
- In ice-free regions, opal burial increases with increasing silicic acid

Correspondence to:
Z. Chase,
Zanna.Chase@utas.edu.au

Citation:
Chase, Z., K. E. Kohfeld, and K. Matsumoto (2015), Controls on biogenic silica burial in the Southern Ocean, *Global Biogeochem. Cycles*, *29*, 1599–1616, doi:10.1002/2015GB005186.

Received 7 MAY 2015
Accepted 3 SEP 2015
Accepted article online 7 SEP 2015
Published online 5 OCT 2015

Controls on biogenic silica burial in the Southern Ocean

Zanna Chase[1], Karen E. Kohfeld[2], and Katsumi Matsumoto[3]

[1]Institute for Marine and Antarctic Studies, University of Tasmania, Hobart, Tasmania, Australia, [2]School of Resource and Environmental Management, Simon Fraser University, Burnaby, British Columbia, Canada, [3]Department of Earth Sciences, University of Minnesota, Minneapolis, Minnesota, USA

Abstract Understanding the controls on opal export in the Southern Ocean can inform both the prediction of how the leakage of silicic acid from the Southern Ocean responds to climate and the interpretation of paleo-proxies. We have compiled a database of 185 ^{230}Thorium-normalized opal burial rates and 493 opal concentration measurements in Southern Ocean sediments and matched these with environmental climatologies. By subdividing the Southern Ocean on the basis of oceanographic regions and interpolating the opal burial rates, we estimate a total biogenic Si burial south of 40°S of 2.3 ± 1.0 Tmol Si yr^{-1}. In both the seasonally ice-covered and permanently ice-free regions we can explain 73% of opal burial variability from surface ocean properties. Where sea ice is present for at least part of the year, the length of the ice-free season determines the upper limit of opal burial in the underlying sediments. In the ice-free regions of the Southern Ocean, the supply of silicic acid through winter mixing is the most important factor. Our results do not support a strong role of iron in controlling opal burial. We do however find that satellite-derived net primary production increases with increasing (modeled) dust delivery. These findings support the decoupling between carbon and opal fluxes in the Southern Ocean. When corrected for opal dissolution, the observed opal fluxes are in reasonable agreement with fluxes simulated using an ocean biogeochemical model. However, the results suggest current preservation algorithms for opal could be improved by incorporating the composition of particle flux, not only its magnitude.

1. Introduction

Close to half of the ocean's biogenic silica, or opal, burial occurs in sediments of the Southern Ocean [*DeMaster*, 2002]. Upwelling of deep water brings large amounts of silicic acid to the surface where it is converted to biogenic Si primarily by diatoms. The Southern Ocean zone of diatom production is reflected in the underlying sediments in the form of the "opal belt" [*Lisitzin*, 1971], a circumpolar band of opal-rich sediments. Upwelled silicic acid not consumed in the Southern Ocean is exported to the low latitude thermocline via mode and intermediate waters [*Sarmiento et al.,* 2004], where it can support diatom production. The magnitude of silicic acid export to the low latitudes therefore depends on both the rate of supply of silicic acid through upwelling and on the degree of utilization of silicic acid by diatoms in the Southern Ocean. In the modern Southern Ocean, Si utilization is efficient, with the Southern Ocean acting as a net sink for Si [*Tréguer,* 2014]. This results in Si-depleted waters feeding the tropical thermocline and favoring growth of $CaCO_3$-bearing phytoplankton such as coccolithophores over diatoms in the low latitudes [*Matsumoto et al.,* 2014; *Sarmiento et al.,* 2004]. According to the silicic acid leakage hypothesis (SALH) [*Brzezinski et al.,* 2002; *Matsumoto et al.,* 2002], the export, or leakage, of silicic acid from the Southern Ocean increased during glacial times. The leakage may have occurred in response to either increased iron delivery from dust, decreasing the Si:N uptake ratio of diatoms [*Takeda*, 1998], or an increase in sea ice, decreasing Si uptake in the Antarctic zone [*Chase et al.,* 2003; *Kienast et al.,* 2006; *Matsumoto et al.,* 2014]. In either case, the resulting shift away from carbonate-bearing phytoplankton in the low latitudes would decrease the $CaCO_3$:organic C rain ratio, leading to ocean uptake of atmospheric CO_2 [*Archer et al.,* 2000]. The SALH therefore proposes that the degree of Si utilization in the Southern Ocean can modulate atmospheric CO_2.

The motivation for this study is to better understand what determines, at the large scale, the production and export of biogenic Si in the Southern Ocean. Is biogenic Si export determined primarily by the supply of silicic acid via upwelling? Alternatively, is biogenic Si export smaller than the rate of supply of silicic acid and capped by a predictable environmental constraint such as light availability? How does iron availability modulate

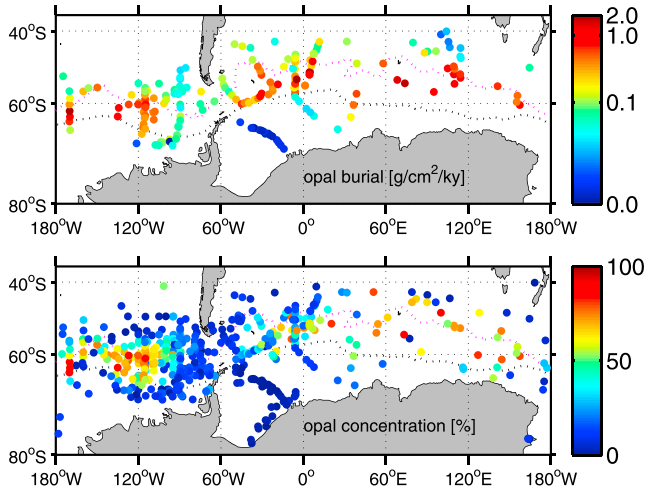

Figure 1. Spatial distribution of ^{230}Th-normalized sedimentary (top) opal burial and (bottom) opal concentration measurements compiled for this study. ^{230}Th-normalized opal burial data are from *Bradtmiller et al.* [2009], *Chase et al.* [2003], *Dezileau et al.* [2003], *Frank et al.* [1999, 2000], *Geibert et al.* [2005], *Kumar* [1994], *Pondaven et al.* [2000], *Yu* [1994], and L. Burckle (unpublished opal concentration data), and are archived at PANGEA (http://issues.pangaea.de/browse/PDI-9945). The location of the Antarctic Polar Front is indicated in pink, and the mean location of the November ice edge is indicated in black (mean 1979–2007 from the Australian Antarctic Data Centre, https://www1.data.antarctica.gov.au/).

biogenic Si export? Understanding the controls on biogenic Si export will inform (a) the prediction of how the leakage of silicic acid from the Southern Ocean might respond to climate change (past and future) and (b) the interpretation of paleo-proxies. For example, sedimentary opal has been used as a proxy for sea-ice extent [*Cooke and Hays*, 1982], productivity [*Mortlock et al.,* 1991], and upwelling intensity [*Anderson et al.,* 2009]. This study also provides an updated estimate of the overall magnitude of biogenic silica burial in Southern Ocean sediments, useful for global budgeting.

We take an empirical approach to investigate the environmental controls on biogenic Si export. We use surface sediment as a recorder of "recent" biogenic Si burial, determined from measurements of ^{230}Th-normalized opal burial. Under ideal conditions, surface sediments can be thought of as analogous to bottom-mounted sediment traps. By integrating over the seasonal cycle and capturing the composition of export flux, sediment traps provide important information on the controls on annual biogenic Si flux in the Southern Ocean [*Honjo et al.,* 2000; *Nodder et al.,* 2005; *Trull et al.,* 2001a]. However, the number of sediment trap deployments in the Southern Ocean is very limited. To the extent that surface sediments act as sediment traps, integrating flux over thousands of years, these more numerous archives can contribute to an understanding of the environmental controls on biogenic Si export, recognizing of course the potential for decoupling between surface processes and seafloor fluxes. We use ^{230}Th normalization to correct for postdepositional sediment redistribution [*Francois et al.,* 2004], which can be significant in the Southern Ocean [*Dezileau et al.,* 2000]. This approach was first applied in the Southern Ocean by *DeMaster* [2002] and subsequently by *Geibert et al.* [2005]. Indeed, we have used and extended the data set of *Geibert et al.* [2005]. Here we have associated every surface sediment opal flux estimate with corresponding climatological values for putative environmental drivers of opal flux: surface silicic acid concentrations, ice cover, mixed layer depth, and dust deposition. Th normalization cannot account for opal that has dissolved prior to burial, and the fluxes calculated using Th normalization are therefore often referred to as "preserved vertical fluxes." Here we will refer to Th-normalized opal flux as simply "opal burial." We have also analyzed a much larger data set of Southern Ocean sedimentary opal concentrations. The interpretation of opal concentration is complicated, as it reflects both the magnitude of sedimentary opal burial and its dilution by the flux of other sedimentary phases. Nevertheless, we include this parameter as many more measurements of opal concentration are available.

2. Methods

2.1. Surface Sediment Data Compilation: ^{230}Th-normalized Opal Burial and Opal Concentration

We assembled from the literature 185 Th-normalized opal burial measurements from surface sediments of the Southern Ocean (defined as south of 40°S) (Figure 1 and Table 1). The majority of the measurements (111) are from *Geibert et al.* [2005], with the remainder from eight other publications [*Bradtmiller et al.,* 2009; *Chase et al.,* 2003; *Dezileau et al.,* 2003; *Frank et al.,* 1999, 2000; *Kumar,* 1994; *Pondaven et al.,* 2000; *Yu,* 1994] that extend the geographic coverage into the SW Pacific and Indian oceans. We also compiled a total of 493 opal concentration measurements (Figure 1), largely composed of measurements made at

Table 1. Mean, Standard Deviation, and Number of Observations of Opal Burial and Opal Concentration in Four Regions of the Southern Ocean

	Opal Burial (g cm^{-2} kyr^{-1})			Opal Concentration (Dry Weight %)		
	Mean	Stdev	*n*	Mean	Stdev	*n*
Pacific	0.25	0.30	78	32	25	276
Atlantic/Indian	0.32	0.40	107	25	24	217
N APF[a]	0.19	0.22	80	29	24	177
S APF	0.37	0.42	105	28	25	316

[a]North of the Antarctic Polar Front (APF) in all sectors.

LDEO (L. Burkle, pers. comm., 2005). While the core tops used by *Geibert et al.* [2005] were not explicitly dated, the authors took care to only include the undisturbed surface-most sediment layer and did not include any samples collected by gravity or piston core. Here we have included samples collected by gravity and piston corer, but all of the cores have some form of stratigraphic control, such that surface sediments in the ^{230}Th compilation are known to be of Holocene age (<10 ka). Samples with opal concentration alone (e.g., 327 samples) have not been assessed for age control and are presented as simply "surface sediments." Where necessary, data were converted to g cm^{-2} kyr^{-1}, assuming a molecular weight for opal of 67.3 g mol^{-1} [*Mortlock and Froelich*, 1989]. The full data set is archived at the earth science archiving site PANGAEA (http://issues.pangaea.de/browse/PDI-9945).

2.2. Environmental Climatologies

The environmental climatologies used are summarized in Table 2. The season length is defined as the number of ice-free days per year, based on a 15% ice-cover threshold to define the presence of sea ice [*Stammerjohn et al.,* 2008]. Spatial patterns of ice-season length are very similar regardless of ice concentration threshold, from 15% to 50% [*Parkinson,* 1994]. Dust deposition, which we treat here as a proxy for eolian iron deposition, is from a global model of pre-industrial dust deposition [*Mahowald et al.,* 2006]. In treating dust as a proxy for eolian iron, we assume that both the iron content of dust and the fraction of iron in dust that is soluble are constant. For each opal flux and opal concentration data point we performed a simple match-up with the gridded environmental climatologies. No spatial averaging of environmental parameters was applied. The Antarctic Polar Front (APF) [from *Orsi et al.,* 1995] position for each sediment site was expressed as degrees north of the latitude of the APF at that longitude. The additional variables of water depth and total flux (from ^{230}Th) were also examined because they could impact opal preservation (and therefore also opal burial). While the total mass accumulation rate might be expected to govern opal preservation more than vertical rain rate, we have used total Th-normalized burial as this parameter is available from a much larger fraction of the cores examined.

2.3. Si Burial Calculation and Bioregionalization

Th-normalized burial rates are useful for constraining the sediment burial term in the global Si budget. A method is needed to extrapolate the sparse measurements to the entire Southern Ocean. In their study of Th-normalized opal burial in the Atlantic and SE Pacific sectors, *Geibert et al.* [2005] used the classical

Table 2. Environmental Climatologies Used to Match Up With Seafloor Opal Data

Variable	Data Set	Years	Source	Grid Size
Ice-free season length	Sea ice trends and climatologies from SMMR and SSM/I bootstrap algorithm	1979–2006	NSIDC *Stroeve* [2003], *Stammerjohn et al.* [2008]	25 km
Nutrients	WOA09, monthly objectively interpolated, 0–30 m	1970–2008	NODC	1°
Mixed layer depth	MLD_DR003, IsoPycnal layer depth, monthly	1961–2008	Locean-ipsl	2°
Dust deposition	Modeled global dust	Pre-industrial "composite"	*Mahowald et al.* [2006]	2°
Sea surface temperature	In situ and satellite SST climatology	1961–1990	*Reynolds et al.* [2002]	1°
Antarctic Polar Front	From ship-based hydrographic data	1961–1990	*Orsi et al.* [1995]	NA
Net primary production	CbPM using SeaWiFS r2010	1998–2010	*Westberry et al.* [2008]	1°

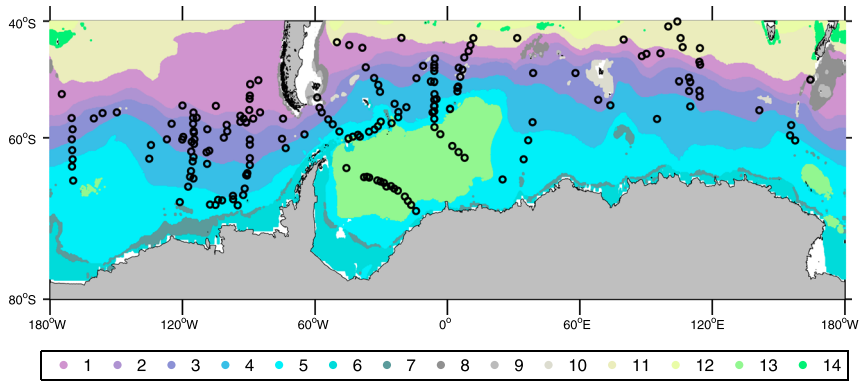

Figure 2. The location of surface opal flux measurements shown on a map of objectively classified bioregions of the Southern Ocean, from *Grant et al.* [2006]. 1. Southern Temperate; 2. Sub-Antarctic front; 3. Polar Front; 4. Southern ACC front; 5. Antarctic Open Ocean; 6. Antarctic Shelves; 7. Antarctic Shelf Slope, BANZARE Bank; 8. Campbell Plateau, Patagonian Shelf, Africana Rise; 9. Inner Patagonian Shelf, Campbell and Crozet islands; 10. Kerguelen, Heard and McDonald islands; 11. Subtropical Front; 12. Northern temperate; 13. Weddell Gyre and Ross Sea banks; 14. Chatham Rise.

sea-ice-based zonation of the Southern Ocean [*Treguer and Van Bennekom*, 1991] as the basis for extrapolation. Here we use a more recent bioregionalization effort for the Southern Ocean [*Grant et al.,* 2006] (Figure 2 and Table 3), which uses a clustering algorithm to subdivide the Southern Ocean into 14 regions on the basis of bathymetry, sea surface temperature (SST), surface nitrate concentration, and surface silicic acid concentration. This regionalization classified 96% of the ocean area south of 40°S, with some coastal areas missing due to lack of data (Table 3). All of the opal burial data lie within classified regions. Six of the regions contain no opal burial measurements, but these regions combined comprise only 6% of the classified area south of 40°S (Table 3). For each region with at least two measurements of Th-normalized Si burial a mean and standard deviation were calculated. The mean Si burial per square meter was then multiplied by the region area to obtain a total burial per region. For the regions with no data we assigned a Si burial rate based on the burial rate in the next most similar region, based on the clustering output [*Grant et al.,* 2006] (see Table 3). For these

Table 3. Bioregions [*Grant et al.,* 2006] and Associated Mean and Standard Deviation of Th-normalized Opal Burial Estimates Used to Calculate the Total Burial of Biogenic Si in Sediments South of 40°S[a]

Region Name	Area (10^6 km^2)	Fractional Area	Opal Burial n	Samples per km^2	Mean Opal Burial [g/cm^2/kyr]	Std Opal Burial [g/cm^2/kyr][b]	Mean Si Burial [10^9 mol/yr]	Std Si Burial [10^9 mol/yr]
1. Southern Temperate	14.21	0.19	21	113	0.06	0.04	132.6	91.9
2. Sub-Antarctic front	4.79	0.06	16	256	0.09	0.04	62.4	28.0
3. Polar Front	9.30	0.12	50	413	0.38	0.32	530.2	444.2
4. Southern ACC front	10.95	0.14	43	301	0.53	0.49	868.0	798.3
5. Antarctic Open Ocean	10.94	0.14	27	189	0.30	0.27	490.6	433.7
6. Antarctic Shelves	1.91	0.02	0	0	0.04[c]	0.04	11.3	11.3
7. Antarctic Shelf Slope, BANZARE Bank	0.43	0.01	0	0	0.04[c]	0.04	2.6	2.6
8. Campbell Plateau, Patagonian Shelf, Africana Rise	0.94	0.01	1	82	0.11	0.11	15.9	15.9
9. Inner Patagonian Shelf, Campbell and Crozet islands	0.11	0.00	0	0	0.11[d]	0.11	1.9	1.9
10. Kerguelen, Heard, and McDonald islands	0.28	0.00	0	0	0.09[e]	0.09	3.9	3.9
11. Subtropical Front	13.16	0.17	8	47	0.06	0.07	119.0	136.7
12. Northern temperate	1.46	0.02	0	0	0.06[f]	0.06	13.6	13.6
13. Weddell Gyre and Ross Sea banks	4.56	0.06	20	336	0.04	0.13	28.4	91.1
14. Chatham Rise	0.43	0.01	0	0	0.11[d]	0.11	7.3	7.3

[a]Regions without opal burial data were assigned an average opal burial equal to that in a "comparable" region (subjectively chosen).
[b]Regions with no data were assigned a standard deviation of 100%.
[c]Assumed same as region 13.
[d]Assumed same as region 8.
[e]Assumed same as region 2.
[f]Assumed same as region 11.

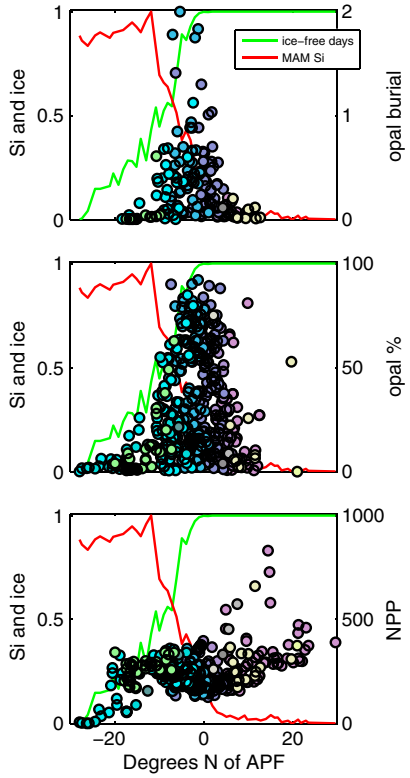

Figure 3. (top) Opal burial (in g/cm^2/kyr), (middle) opal concentration, and (bottom) satellite-derived net primary production (NPP, in mg/m^2/d) [from *Westberry et al.,* 2008] as a function of the latitude of the site relative to the local mean position of the Antarctic Polar Front (APF) [from *Orsi et al.,* 1995]. Also plotted are the zonally averaged values of season length (number of ice-free days) and silicic acid availability (MAM surface silicic acid concentration). These parameters have been normalized to a range of 0–1. Data points are color coded by bioregion (Figure 2).

regions and for the Campbell Plateau region with only a single Si burial measurement, we assigned a standard deviation equal to 100% of the Si burial value.

3. Results

The classical opal belt [*Lisitzin*, 1971] is reproduced in the updated data set in the spatial distribution of Th-normalized opal burial (Figure 1a) and opal concentration (Figure 1b). Viewed as a function of the zonal distance from the APF, the data show a maximum in opal burial and opal concentration in the vicinity of the Polar Front (Figure 3). Indeed, within the resolution of these data, the zonal maxima of both opal burial and opal concentration are centered on the APF. Qualitatively, the spatial distribution of opal flux, and to a lesser degree opal concentration, is consistent with the zonal averages of season length (number of ice-free days per year) and silicic acid availability: decreasing opal burial to the south tracks the decreasing season length, while increasing opal burial to the north tracks increasing silicic acid availability. The intersection of minimum ice-season length and maximum silicic acid availability is on average about 5° south of the APF, which is south of the maximum in opal burial and concentration (Figure 3). Net primary productivity (NPP) at the same locations shows a different spatial pattern (Figure 3), with relatively little variability as a function of latitude except in the far south where NPP decreases as sites are ice covered more than 6 months of the year.

We compare (Figure 4) the observed opal burial rates with modern opal fluxes to the seafloor simulated using MESMO2, an earth system model of intermediate complexity [*Matsumoto et al.,* 2008, 2013]. The model has a prognostic export production of organic carbon, opal, and $CaCO_3$ with dependencies on colimitation by multiple nutrients (P, N, Si, and Fe), light, temperature, and mixed layer depth. Opal export is related to organic carbon export by the Si:N uptake ratio of diatoms, which is a function of Fe availability. This data-model comparison shows a broadly similar distribution of opal flux to the seafloor as a function of latitude as the observations of Th-normalized opal burial (Figure 4). Specifically, in MESMO2 as in the observations, opal fluxes show a midlatitude maximum. However, the latitude of maximum opal flux is about 5° farther south in the observations compared to the model. MESMO2 output shown in Figure 4 has been shifted south by 5°. We suspect the latitudinal offset of the MESMO2 output is because the APF in MESMO2 is located too far north, due to the coarse model resolution. The latitudinal resolution of MESMO2 is uniform in sine of latitude so that it becomes coarser toward the poles; it is 5–7° near the APF. Other model-data comparisons support the notion that the APF in MESMO2 is too far north. First, the MESMO2 estimate of Antarctic sea ice during September 2000 is 50–75% greater than the satellite-derived estimate [*Matsumoto et al.,* 2013]. As the APF is the northerly limit of sea ice, this is consistent with the APF in MESMO being too far north. Second, in MESMO2 the subsurface Si* minimum is sourced from the surface at approximately 45°S, whereas in the observations it is close to 50°S [*Matsumoto et al.,* 2013]. If we assume the subsurface Si* minimum

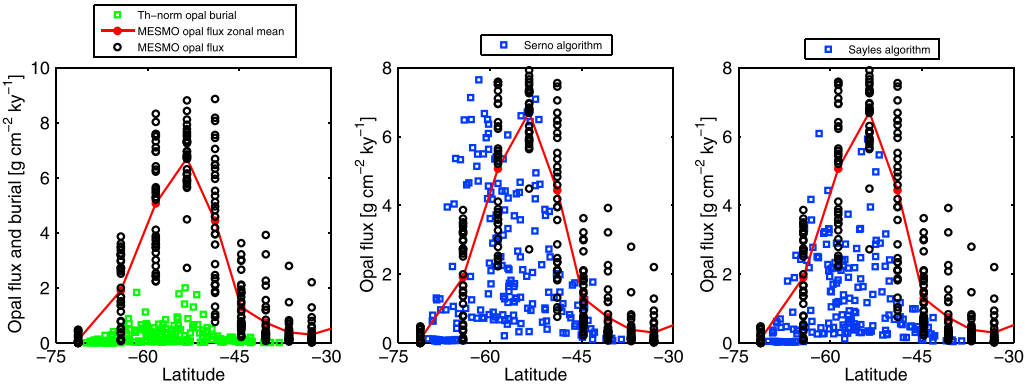

Figure 4. (left) MESMO2 [*Matsumoto et al.,* 2013] modeled opal flux to the seafloor compared to Th-normalized preserved opal burial. (middle) MESMO2 modeled opal flux to the seafloor compared to opal flux to the seafloor derived by correcting Th-normalized preserved opal burial for dissolution at the seafloor using the algorithm of *Serno et al.* [2014]. (right) MESMO2 modeled opal flux to the seafloor compared to opal flux to the seafloor derived by correcting Th-normalized preserved opal burial for dissolution at the seafloor using the algorithm of *Sayles et al.* [2001]. In all plots the MESMO2 output has been shifted south by 5°.

corresponds to the location of the APF [*Sarmiento et al.,* 2004], this supports the conclusion that the model's APF is about 5° too far north.

MESMO2 calculates the vertical rain of opal to the seafloor, while Th-normalized fluxes record the preserved, buried opal rain, after post-depositional dissolution. Between 60% and 96% of the opal rain to the seafloor is dissolved prior to burial [*Ragueneau et al.,* 2002]. In order to directly compare the observations with the model, we have accounted for postdepositional dissolution using two published empirical algorithms. The algorithm of *Serno et al.* [2014] was developed based on a comparison between sediment trap and seafloor opal burial fluxes in the North Pacific, and derives opal rain by scaling opal burial by an inverse linear function of the total (Th-based) mass accumulation rate. The algorithm of *Sayles et al.* [2001] is also based on a sediment trap-seafloor comparison, but for the Southern Ocean, and derives opal rain by scaling opal burial by an inverse function of the square root of the sedimentation rate. When applied to our opal burial data, both algorithms produce opal fluxes to the seafloor within the range of the MESMO predictions, with the observations being slightly higher relative to the model output in the southern part of the domain (Figure 4). To the degree that MEMSO accurately simulates opal export, which compares reasonably well to available observations [*Matsumoto et al.,* 2013], the data-model comparison indicates that the large scale features of opal export in the modern ocean are captured by this compilation of opal burial rates.

In order to identify additional environmental controls on opal burial, we next separated the data into those sites with more or less than seven ice-covered days per year. The results were not sensitive to the choice of minimum ice-cover durations of between 0 and 10 ice-covered days per year to define the ice-affected region. A cutoff of seven ice-covered days produced the best fit with environmental variables in both the ice-covered and ice-free regions. The number of ice-free days appears to impose an upper limit on the opal burial to the underlying sediment (Figure 5, left). When the ice-free season is shorter than about 200 days, there is essentially no opal burial. For longer ice-free seasons, the maximum realized opal burial increases with increasing number of ice-free days, although very low opal burial is possible irrespective of ice-season length (Figure 5, left). The relationship between opal concentration and season length (Figure 5, right) is similar, although without the appearance of a threshold ice-free season length. Rather, maximum

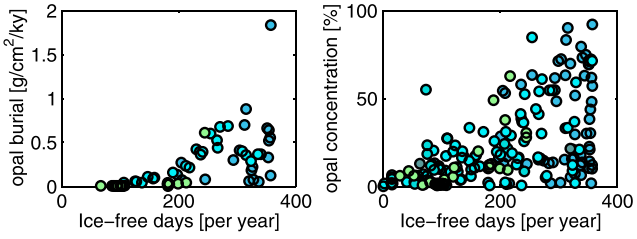

Figure 5. (left) Opal burial and (right) opal concentration as a function of the number of ice-free days per year, for sites where is ice present (15% coverage) for at least 7 days per year. Data points are color coded by bioregion (Figure 2).

Table 4. Details of Statistical Comparisons Discussed in the Text[a]

Dependent Variable	Region	Predictor Variables	RMSE	Adjusted r^2	n	p
Log opal burial	Ice covered	Dust	0.74	0.19	66	0.0001
Log opal burial	Ice covered	Annual SST	0.51	0.62	66	<0.0001
Log opal burial	Ice covered	Season	0.46	0.69	67	<0.0001
Log opal burial	Ice covered	Total flux	0.63	0.43	66	<0.0001
Log opal burial	Ice covered	MAM_MLD	0.67	0.34	67	<0.0001
Log opal burial	Ice covered	*Season, total flux, MAM_MLD*	0.43	0.73	66	<0.0001
Log opal burial corrected Sayles	Ice covered	Season, MAM_MLD	0.43	0.66	66	<0.0001
Log opal burial corrected Serno	Ice covered	Season, MAM_MLD	0.43	0.61	66	<0.0001
Log opal burial	Ice free	Dust	0.53	0	118	**0.815**
Log opal burial	Ice free	SON_Si	0.41	0.39	118	<0.0001
Log opal burial	Ice free	Total flux	0.46	0.22	114	<0.0001
Log opal burial	Ice free	MAM_MLD	0.53	0.004	118	**0.22**
Log opal burial	Ice free	JJA_sst	0.4	0.44	118	<0.0001
Log opal burial	Ice free	SON_sst (–)	0.39	0.47	118	<0.0001
Log opal burial	Ice free	*Total flux, MAM_MLD, dust, JJA_sst, SON_sst (–)*	0.27	0.73	114	<0.0001
Log opal burial	Ice free; minimal frontal movement	Total flux, MAM_MLD, dust, JJA_sst, SON_sst (–)	0.24	0.72	59	<0.0001
Log opal burial	Ice free	NPP	0.382	0.0131	118	**0.113**
Log opal burial corrected Sayles	Ice free	MAM_MLD, dust, JJA_sst, SON_sst (–)	0.28	0.65	114	<0.0001
Log opal burial corrected Serno	Ice free	MAM_MLD, dust, JJA_sst, SON_sst (–)	0.28	0.63	114	<0.0001
Ice-covered days per year	Ice covered	Opal burial (–), annual SST	30.9	0.89	66	<0.0001
Ice-covered days per year	Ice covered	Annual SST	33.5	0.88	66	<0.0001
NPP	Ice free	Dust	57	0.61	347	<0.0001

[a]Where predictor variables are shown in *italics* the choice of variables was determined from a stepwise multiple linear regression procedure from the list of variables in Table 2. Nonsignificant ($p > 0.0001$) correlations are in bold.

opal concentration increases from 0% to >90% as the ice-free season increases from 0 days to year-round. Sedimentary opal concentration is determined by the burial rate of opal relative to other constituents. The difference between opal concentration and opal burial as a function of ice-free days (Figure 5) can be explained if total particle rain increases with increasing season length more slowly than opal rain increases with season length. In other words, at high southern latitudes the small total particle flux is dominated by Si-producing organisms such that opal % is high while opal burial is low. Such a model is consistent with sediment trap records of particle flux from the SW Pacific [*Honjo et al.,* 2000; *Sayles et al.,* 2001]. Differences in opal preservation with season length may also contribute to the contrast between opal burial and opal concentration, but are not necessary to explain the contrast.

In the seasonally ice-covered region ($n = 66$) a stepwise multiple linear regression identified the number of ice-free days, the average autumn (March, April, and May) mixed layer depth (MLD), and total flux (Th-normalized) as explanatory variables, together accounting for 73% of the variability in (log normalized) opal burial (adjusted $r^2 = 0.73$, Table 4). Considered independently, all three variables make a positive contribution to opal burial, increasing in importance from MLD < total flux < ice-free days (Table 4).

In the ice-free region ($n = 114$), multiple linear regression identified six predictive variables, which combine to explain 73% of the variability in opal flux (Table 4): total flux, average autumn MLD, dust flux, winter SST (June, July, and August), and spring SST (September, October, and November). All variables except spring SST make a positive contribution to opal flux. Considered on their own (and therefore ignoring the impact of likely colinearity), SST and total flux explain the most variability, with dust and MLD making minor contributions (Table 4). Figure 6 shows the spatial patterns of areas where this statistical model over-predicts (red dots) and under-predicts (blue dots) opal burial. Predictions are generally more accurate in the northern part of the domain, with a hint of under-prediction in the eastern side of the basins (Figure 6, top). In contrast, the predictions of the multiple linear regression in the ice-affected region are generally more accurate to the south, where there is greater ice cover (Figure 6, bottom). Therefore, in both the ice-affected and ice-free regions the model predictions are least accurate in the transition zone between ice-affected and ice-free zones. A possible explanation for this is that the opal burial reflects relict conditions from a period when ice extent was different from today [e.g., *Curran et al.*, 2003].

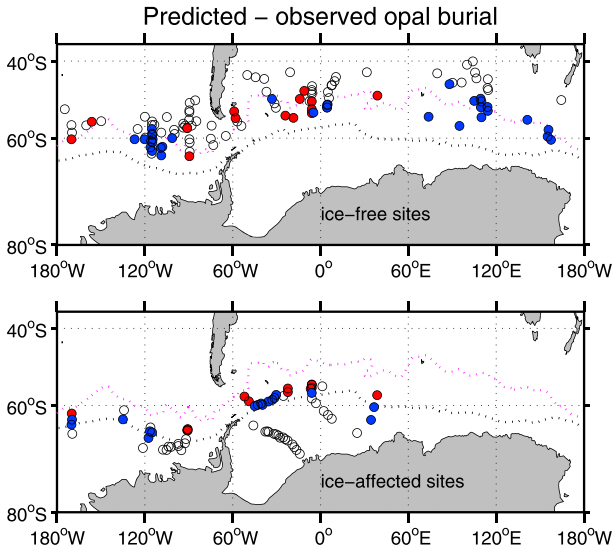

Figure 6. Accuracy of the multiple linear regression predictions of opal burial at the (top) ice-free and (bottom) ice-affected sites. White dots indicate sites where predicted and observed opal burial agree to within 0.1 g/cm^2/kyr, red dots indicate where predicted opal burial is greater than observed opal burial by more than 0.1 g/cm^2/kyr, and blue dots where predicted opal burial is less than observed opal burial by more than 0.1 g/cm^2/kyr.

Considering the difference in time-averaging between the climatologies (decades) and the surface sediment records (hundreds to thousands of years), we were concerned that changes in frontal positions over these timescales may have obscured some of the correlations between environmental variables and seafloor properties. We therefore repeated our analysis of ice-free sites considering only the region from 180°E to 315°E in the Atlantic, where frontal positions have moved the least over the past 15 years [*Sokolov and Rintoul*, 2009]. The correlations between opal burial and environmental variables were essentially the same when considering this more restricted area ($n = 59$) where changes in frontal position were likely small (Table 4).

Although NPP is not strictly an environmental driver of biogenic opal production, NPP and biogenic opal burial could be correlated, particularly if diatoms dominate NPP. We were therefore interested in whether there is a relationship between sedimentary opal burial and primary production. We found none (Figure 7, left). We did, however, find a significant correlation between NPP and dust flux (Figure 7, middle; $r^2 = 0.62$). We also tested the relationship between dust and productivity using the standard SeaWiFS product, as well as the *Johnson et al.* [2013] chlorophyll algorithm for the Southern Ocean, and found much weaker ($r^2 = 0.38$ and 0.22, respectively) but still statistically significant correlations.

Using a bioregionalization approach (Table 3) we estimate the total burial of biogenic Si in sediments south of 40°S to be 2.3 ± 1 Tmol yr^{-1}. The Southern Antarctic Circumpolar Current (ACC) front, Polar Front, and Antarctic Open Ocean regions have the largest Si burial per unit area and also account for the most Si burial south of 40°S; together they account for 82% of the Si burial. The mean per-area flux is largest in the Southern ACC front region (0.53 g cm^{-2} kyr^{-1}). Because of their large area, the Southern Temperate and Subtropical Front regions also contribute significantly (combined 5.5% of total) to Si burial in the Southern Ocean, despite their small per-area average fluxes (0.06 g cm^{-2} kyr^{-1} in both regions).

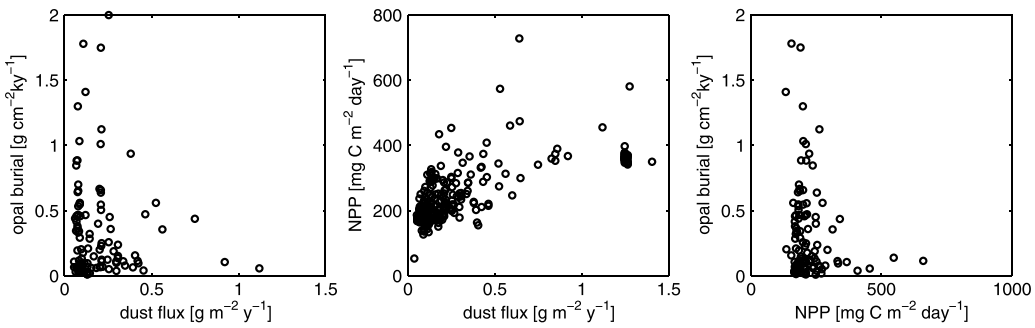

Figure 7. Scatter plots of (left) opal burial versus dust flux [*Mahowald et al.*, 2006], (middle) satellite-derived net primary production (NPP) [*Westberry et al.*, 2008] versus dust flux, and (right) opal burial versus NPP at sites where there is sea-ice present less than 7 days per year.

4. Discussion

The opal belt was initially defined on the basis of sedimentary opal concentration [*Lisitzin*, 1971], and then diatom preservation [*Burckle and Cirilli*, 1987], opal accumulation rate [*DeMaster*, 1981], and more recently Th-normalized opal flux [*DeMaster*, 2002; *Geibert et al.,* 2005; this work]. The southern limit of the opal belt has long been attributed to the presence of sea ice suppressing annually averaged diatom production. Indeed, on the basis of this modern distribution, the opal belt has been suggested as a proxy for the summer [*Cooke and Hays,* 1982] or spring [*Burckle and Cirilli*, 1987] ice edge. Dilution by ice-rafted debris may also contribute to defining the southern boundary of the opal (concentration) belt [*Sayles et al.,* 2001].

The northern boundary of the opal belt was initially attributed to a temperature limitation on diatom growth, closely tied to the location of the Sub-Antarctic Front [*Burckle and Cirilli*, 1987]. More recent work attributes low diatom abundance north of the APF, and by implication the northern limit of the sedimentary opal belt, to low concentrations of silicic acid [*Trull et al.,* 2001b]. In support of silicic acid limitation, research from 170° W has shown that diatom growth at ice-free latitudes effectively consumes all available silicic acid on a seasonal basis [*Nelson et al.,* 2002; *Sigmon et al.,* 2002], leading to the suggestion that opal flux can be used as a proxy for silicic acid supply in the geological record [*Anderson et al.,* 2009]. In the following we discuss the new insights provided by this updated map of biogenic Si burial, followed by a discussion of the revised Si burial term for the Southern Ocean.

4.1. Southern Control: The Role of Sea-Ice

The role of sea-ice in reducing productivity has been invoked by paleoceanographers to explain variability of Antarctic opal burial records on glacial to interglacial timescales [*Charles et al.,* 1991; *Chase et al.,* 2003]. Our data show that the length of the ice-free season places an upper limit on opal burial. This is consistent with the results of *Chase et al.* [2003], who noted a correspondence between the decreasing opal flux in surface sediments south of 61°S along 170°W and the decreasing number of ice-free days. Here we confirm this relationship across the whole of the Southern Ocean, using a much larger and circumpolar opal burial data set, a better representation of the ice-season length, and a more quantitative matching procedure. This larger data set shows that although ice places an upper limit on opal burial, other factors are also important, and in many locations, opal burial is much lower than the "upper limit" imposed by the length of the ice-free season. Reductions in opal burial in the sediment record cannot be taken alone as evidence of sea-ice expansion but should ideally be coupled with additional proxies of sea-ice change, as discussed below.

On an annual basis, increases in the duration of sea-ice cover lead to a decrease in the maximum burial of biogenic silica that can be expected, presumably by decreasing annual diatom productivity through light limitation induced by ice cover. Diatoms are a dominant component of the phytoplankton community in the seasonally ice-covered region of the Southern Ocean, so we might expect annual carbon export to also decrease with increasing duration of ice cover. Indeed, satellite-derived NPP decreases with increasing ice duration (Figure 3), suggesting that annual carbon export is also limited by the length of the growing season, at least when ice is present more than 6 months a year. This conclusion is complicated by the poor satellite data coverage at high southern latitudes and the possible ephemeral nature of ice-edge blooms. However, MESMO2 output reproduces a similar pattern, with particulate organic carbon (POC) flux to the seafloor decreasing with latitude (increasing ice duration), in the far south of the model domain. A compilation of in situ productivity measurements in the Arctic shows a remarkably similar regulation of annual pelagic primary production and the open water season [*Rysgaard et al.,* 1999]. Thus, although the sea-ice ecosystem and ice-edge blooms can be highly productive, particularly for diatoms, and critical habitat for diverse Antarctic species [*Arrigo*, 2014], on an annual basis, increases in ice duration are associated with decreases in both NPP and opal burial. Although we suspect the decrease in annual opal burial and NPP with ice duration is driven by a decrease in the annual light availability as ice increases, other mechanisms are possible. For example, given the importance of ice-edge blooms, it may be that the timing of ice growth and retreat is critical, relative to other seasonal forcing such as day length and nutrient availability. The ecological makeup of ice-edge blooms, and the nature of the opal produced, may even be affected by the length and phenology of seasonal ice cover.

4.2. Northern Control: The Role of Silicic Acid

At latitudes with negligible sea-ice, the prevailing view is that annual diatom production is determined by silicic acid availability [e.g., *Sigmon et al.,* 2002; *Trull et al.,* 2001b]. Indeed, we find the latitudinal distributions

of opal burial and sediment opal % are consistent with a role of silicic acid availability in determining opal burial, with a northward decrease in opal burial and concentration coincident with a northward decrease in silicic acid concentration (Figure 3). When we compare opal burial with individual climatological variables (Table 3), we find that silicic acid availability at the start of the growing season (SON) explains 39% of the variability in opal burial. We considered other measures of silicic acid availability, including annual and monthly averages, and none was any more predictive of opal burial. Winter and spring SSTs are actually better (inverse) predictors of opal burial than is spring silicic acid, explaining roughly 45% of variability in opal burial (Table 3). One explanation for this is that temperature serves as a proxy for silicic acid concentration, and given the relative paucity of silicic acid measurements across the Southern Ocean, temperature provides a more accurate representation of available Si. An alternative explanation is that temperature directly affects diatom growth or silicification; covariation of many of the environmental variables considered here makes it difficult to distinguish these alternate explanations. In a multivariate context, in addition to SST, autumn MLD, total Th-normalized flux, and dust flux all contributed to explaining opal flux variability in the ice-free region. A role for silicic acid as a master variable is supported by the inclusion of autumn MLD in the multivariate solution, as deeper winter mixing should deliver greater Si to surface waters at the start of the growing season. The mean MLD shoals at the ice-free sites between winter and summer, from a mean of 177 m in winter, 149 m in autumn, 60 m in spring, and 95 m in summer.

4.3. The Role of Iron

The supply of silicic acid is not the only factor thought to affect biogenic Si production in the Southern Ocean. In situ iron fertilization experiments [*Boyd et al.,* 2000; *Coale et al.,* 2004; *Smetacek et al.,* 2012] and the study of naturally iron-fertilized regions [*Blain et al.,* 2007; *Pollard et al.,* 2009] have demonstrated the stimulating effect of iron addition on phytoplankton production, including diatom production. Modeling [*Fennel et al.,* 2003] and correlative studies [*Moore and Abbott*, 2000; *Cassar et al.,* 2007] have further demonstrated the role of iron in determining annual carbon export in the Southern Ocean, although other work has failed to find correlation between dust and primary production in the Southern Ocean [*Boyd et al.,* 2010; *Le Quéré et al.,* 2002].

In this study we find a significant correlation between annual average NPP and modeled dust deposition but not between dust deposition and opal burial (Figure 7 and Table 4). However, in a multivariate context, dust flux slightly improves the predictability of opal flux, in a positive sense (Table 4). The role of iron in explaining variation in opal export is complex. On one hand, iron is required by diatoms for photosynthesis and nitrogen uptake, and iron addition tends to favor the growth of diatoms over other species [*Armand et al.,* 2008]. On the other hand, the Si:C ratio of diatoms decreases with increasing Fe availability. This decrease in Si:C has been shown to occur as a result of (a) changing morphology of individual species [*Leynaert et al.,* 2004; *Marchetti and Harrison*, 2007] and (b) a shift in diatom community composition, from highly silicified species that thrive under low iron conditions to lightly silicified species that thrive under iron-sufficient conditions [*Assmy et al.,* 2013; *Mosseri et al.,* 2008].

Depending on how diatom carbon production responds to iron availability, and how and why net community Si:C uptake varies with iron availability, an increase in iron availability in an iron-limited region may paradoxically lead to a decrease in biogenic Si production, as diatoms, though stimulated to produce more carbon, shift to lower Si:C uptake ratio. This scenario has been proposed to explain the absence of an opal flux event in the equatorial Pacific during the LGM despite evidence for silicic acid leakage [*Pichevin et al.,* 2009]: the abundant iron from dust decreased diatom Si uptake, such that opal flux was lower despite more abundant silicic acid, a result recently confirmed through modeling [*Matsumoto et al.,* 2014]. The role of iron in regulating both diatom carbon fixation and silicification may also explain why biogenic Si did not increase during the ISENEX iron fertilization experiment, despite clear increases in diatom abundance and carbon export [*Assmy et al.,* 2013; *Smetacek et al.,* 2012]. Likewise, in the naturally iron-fertilized waters of the Kerguelen plateau, biogenic Si production and diatom biomass are not significantly different than in surrounding High Nutrient Low Chlorophyll waters [*Mosseri et al.,* 2008]. The same dual action of iron may be at play in the data considered here, driving the phytoplankton toward either a small, Fe-limited growth of highly silicified diatoms or a more prolific growth of weakly silicified diatoms; the net result may be a lack of correlation between iron and opal production and burial.

One caveat in interpreting these results is that dust flux may be a poor proxy for iron availability. While the good correlation between dust flux and NPP (Figure 7), in a region known to be iron limited, suggests dust

flux is a reasonable proxy for iron availability, non-aeolian sources of iron such as shelf iron, upwelling, and even hydrothermal iron are known to be important in the Southern Ocean [*Tagliabue et al.,* 2014; *Death et al.,* 2014]. We conclude that either iron availability plays a minor role in determining opal burial, because of the competing effects of iron on diatom and community C and Si production, or that iron is possibly important in driving opal export, but such a relationship is not seen here because iron availability in the Southern Ocean is poorly represented by dust flux alone.

4.4. The Role of Opal Preservation

In addition to opal export from surface waters, variable preservation of opal in the water column and sediments may contribute to the variability in Th-normalized opal burial. For example, *Leynaert et al.* [1993] have suggested that in the Weddell Sea, low opal burial and concentrations are driven in part by exceptionally poor opal preservation. Factors identified as affecting the preservation of opal in the sediment include diatom species composition [*Warnock et al.,* 2007], pore-water Al [*Van Cappellen and Qiu*, 1997], sediment accumulation rate [*Sayles et al.,* 2001], and bioturbation [*Ragueneau et al.,* 2001]. We found no correlation between water depth and opal burial, nor did the inclusion of water depth improve multivariate prediction of opal burial. This suggests that variable dissolution in the water column does not significantly affect burial, consistent with previous findings [*Tréguer and De La Rocha*, 2013].

The comparison between simulated opal flux to the seafloor from MESMO2 and reconstructed opal flux from opal burial data (Figure 4) provides further insight into opal preservation at the seafloor. Overall, the agreement is quite good between the model and the observations, after shifting the model output south by 5° and applying the Southern Ocean-specific *Sayles et al.* [2001] algorithm to correct for opal dissolution. However, the dissolution-corrected opal fluxes are somewhat lower than modeled opal flux in the north and somewhat higher than modeled flux in the south, an effect that is more pronounced using the Serno et al. correction (Figure 4). While there are many possible explanations for this latitude-dependent offset, including deficiency in the model simulation, one possibility is that it reflects bias in the preservation algorithm. We have used Th-normalized total flux to estimate opal preservation, but the total mass accumulation rate, which is less readily available, is certainly more relevant to opal preservation [*Serno et al.,* 2014]. Furthermore, the composition, as well as the magnitude, of the total flux may be an important variable. Field and laboratory results find the pore-water Al:Si ratio is an important variable regulating sediment opal dissolution: opal preservation increases as this ratio increases [*Dixit and Van Cappellen*, 2003; *Dixit et al.,* 2001]. If the ratio of detritus to opal in the sedimentary flux is an important determinant of pore-water Al:Si, then high-flux regions of the Southern Ocean, which tend to be dominated by opal [*Sayles et al.,* 2001; *Serno et al.,* 2014], will tend to have lower Al:Si ratios in pore waters, and therefore lower preservation of opal, than expected on the basis of total flux alone. Therefore, in the regions of highest fluxes such as the APF where opal dominates, the preservation algorithm may be over-correcting. We concur with *Sarmiento and Gruber* [2006] that the importance of sedimentation rate on opal preservation needs to be revisited in light of research demonstrating the important role of Al in regulating opal preservation. This is particularly true in the Southern Ocean, which is subject to highly variable inputs of Al, from shelf sediments, ice-rafted debris, sediment redistribution, and dust.

4.5. Implications for Paleo-proxies

As discussed in the Introduction, opal burial in the Southern Ocean has been interpreted in different ways in the literature, as reflecting sea-ice coverage, productivity, and stratification or upwelling. This study has implications for the interpretation of opal burial in the paleo record.

The first important implication is that sea-ice duration constrains the maximum value of opal burial observed. Assuming modern-like Si availability in the Antarctic zone (i.e., high Si concentrations), opal accumulation rates higher than the observed maximum for a given sea-ice cover today most likely point to a longer growing season. However, conversely, reductions in opal burial cannot necessarily be interpreted as an increase in the duration of sea-ice cover. Other factors, most notably reduced deep winter mixing and poor opal preservation, also contribute to low opal burial.

In terms of predictive power, opal burial alone can predict the number of ice-covered days per year to within 103 days (2 × root mean square error of the prediction), while annual SST alone, at the same sites, can predict ice-covered days to within 68 days. The combination of opal flux and SST is only marginally better than SST alone, providing a 95% confidence interval of 62 days, reflecting the colinearity of SST and opal flux ($r^2 = 0.62$).

By comparison, the modern analogue technique applied to diatom assemblages can provide a 95% confidence interval of 24 days [*Crosta et al.,* 1998]. A prediction of ice cover to within 2 months is perhaps more useful than it appears at first. For example, debate in the sea-ice reconstruction community centers around the presence of the winter versus summer ice edge. For a given site, this translates to a difference between a sea-ice cover of 4–6 months (winter only) and 9–12 months (winter and summer). In this sense, opal burial and independent SST reconstructions could be used in concert with proxies based on diatom taxonomy to provide improved spatial constraints on sea-ice cover and duration.

In the ice-free Southern Ocean, Th-normalized opal rain has been used as a proxy for both wind-driven upwelling [*Anderson et al.,* 2009] and reductions in wintertime vertical mixing due to density stratification [*Sigman et al.,* 2004; *Jaccard et al.,* 2013]. The premise for opal burial to serve as such a proxy is that both upwelling and vertical mixing processes supply silicic acid to the surface waters. Conversely, stratification and reduced vertical mixing inhibit its supply. Further, this supply of silicic acid determines the annual production of biogenic Si and its subsequent rain to the seafloor. The work presented here provides general support for opal burial as a proxy of silicic acid availability, in that maximum opal burial coincides with maximum silicic acid concentrations (Figure 3). However, the link to either upwelling or other vertical mixing processes is more indirect in that a number of factors associated with silicic acid availability (temperature and MLD) together explain about 70% of the variability in opal burial in the ice-free regions (see above). In theory, Si supply and upwelling could become uncoupled, for example, if there is a change in subsurface silicic acid concentration. The remaining unexplained 30% of variance in opal burial may be due to many factors, including preservation effects, problems with climatologies, and temporal mismatches between the climatologies and surface sediments.

Regardless of the cause, the moderate predictability and indirect link to upwelling do suggest caution is needed when interpreting opal burial as an upwelling proxy in the absence of careful site-specific calibration. Along 170°W, Joint Global Ocean Flux Study produced detailed seasonal observations of water column Si depletion, biogenic production, and vertical flux [*Nelson et al.,* 2002; *Sigmon et al.,* 2002], which provide strong support for a relationship between Si supply (e.g., via upwelling) and Th-normalized opal burial in this region [*Anderson et al.*, 2009]. It is also important to recognize that the role of sea-ice cannot be ignored. Indeed, our data suggest that even a modest increase in sea-ice-season length of 1–2 months per year can significantly decrease opal burial, and conversely, decreases in sea-ice cover could result in increases in maximum burial (Figure 5). Thus, opal burial records need to be carefully interpreted with respect to changes in sea-ice versus changes in upwelling and other vertical mixing processes, and are best interpreted in the context of multiple proxies.

The fact that more than 70% of the variability in opal burial can be accounted for by environmental drivers associated with opal production in surface waters (e.g., season length, Si, and MLD) further supports the view that opal burial recorded using Th normalization is generally reflective of surface water patterns of opal production, as found in previous regional-scale studies [e.g., *Nelson et al.,* 2002]. However, the lack of correlation between opal burial and NPP (Figures 3 and 7) suggests opal burial is not a good proxy for carbon export. This lack of relationship is seen both across the whole data set and independently in the ice-covered and ice-free regions, and persists when opal burial is corrected for preservation using either the Sayles or Serno approach. The good correlation between dust and NPP (Figure 7, $r^2 = 0.61$; Table 4) in the ice-free region, which is believed to be iron limited [e.g., *Coale et al.,* 2004], provides further validation of the NPP product. Together, these observations suggest the discord between opal burial and NPP reflects a real decoupling between carbon export and Si export, as opposed to a mismatch between a surface water signal (NPP) and a sedimentary signal (Th-normalized opal burial). Our results therefore strongly support the notion of decoupling of carbon and opal export in the Southern Ocean [e.g., *Anderson et al.,* 1998; *Assmy et al.,* 2013; *Honjo et al.,* 2000; *Salter et al.,* 2007]. While opal and organic carbon fluxes become even more decoupled with depth due to preferential remineralization of carbon [*Nelson et al.,* 2002], our results support the view that the spatial decoupling arises at the surface. *Abelmann et al.* [2006] suggest the decoupling arises through an ecological shift from the dominance of the thick-walled, high Si-low C exporting *Fragilariopsis kerguelensis*-type ecosystem in the permanently open ocean zone (analogous the "ice-free" region in this study) to the thin-walled, low Si-high C exporting *Chaetoceros*-type productivity in the seasonal ice zone. An iron-mediated decoupling is seen in the model runs of *Matsumoto et al.* [2014], where iron fertilization increases POC flux, and decreases opal flux in the Southern Ocean. We conclude that opal burial is not an appropriate proxy for carbon export in the Southern Ocean.

4.6. Southern Ocean Opal Burial

This work provides an updated estimate of Holocene Si burial in the Southern Ocean based on Th-normalized measurements (Table 3). Using a bioregionization approach to extrapolate measurements to the entire Southern Ocean, we estimate biogenic Si burial south of 40°S to be 2.3 ± 1.0 Tmol Si yr^{-1}. This is only slightly higher than the recent estimate of 2.0 ± 1.2 from *Tréguer and De La Rocha* [2013] for the "opal belt" as defined by *Lisitzin* [1971]. *Geibert et al.* [2005] use the classification based on sea-ice of *Treguer and van Bennekom* [1991] for their extrapolation of Th-normalized Si burial in the Atlantic sector. *Treguer and De La Rocha* [2013] have based their circum-Antarctic estimate on the work of *Geibert et al.* [2005], together with data points (i.e., not interpolated) from *Pondaven et al.* [2000], *Dezileau et al.* [2003], and *DeMaster* [2002]. The revised estimate provided here benefits from a larger data set and the presumably improved interpolation provided by the bioregionalization approach.

The interpolation could be improved further and provides guidance on which regions are most data poor. Seven of the bioregions have no Th-normalized opal flux estimates (Table 3). Of these, the Antarctic shelves and northern temperate regions have the largest surface area. Shallow water limits the application of Th normalization on the shelves, but there are other estimates of sediment accumulation rate (Pb-210, Pu, and C-14) and biogenic silica accumulation in the shelf environments of the Ross Sea and the Western Antarctic peninsula [e.g., *DeMaster et al.,* 1996]. The bioregionalization itself could also be improved, for example, by including sea-ice and ocean color data, or using alternative statistical approaches [*Grant et al.,* 2006]. We estimate an opal burial efficiency (opal export/burial) south of 40°S of 3.6% from the ratio of opal burial estimated here from observations (2.3 Tmol Si yr^{-1}) to opal export from the mixed layer estimated from MESMO 2 (63.3 Tmol Si yr^{-1}). This opal preservation efficiency is consistent with observation-based estimates from the Southern Ocean, which range from 1% to 6% [*Nelson et al.,* 2002; *Pondaven et al.,* 2000], lending confidence to both the MESMO opal export result and the observationally-constrained opal burial result.

There are biogeochemical implications to the factors limiting opal export. We assume that the link between sea-ice and opal burial arises because sea-ice limits the annual consumption of silicic acid by diatoms, rather than, for example, affecting opal preservation. If this is the case, greater sea-ice extent and duration should lead to reduced silicic acid uptake in the Antarctic zone, leaving more silicic acid available to be transported across the Polar Front and potentially into the low latitude thermocline via mode and intermediate waters [*Sarmiento et al.,* 2004]. In this sense, expanded sea-ice can in theory lead to silicic acid leakage from the Southern Ocean, as demonstrated in a model [*Matsumoto et al.,* 2014]. Likewise, if the length of the ice-free season increases in the future, and opal burial in the Southern Ocean increases as a result, we can speculate that this will result in even greater trapping of Si in the Southern Ocean and more severe Si limitation of diatom growth outside the Southern Ocean.

The sea-ice mechanism for silicic acid leakage has been used to explain large opal fluxes observed [*Hayes et al.,* 2011; *Kienast et al.,* 2006] in the eastern equatorial Pacific during marine isotope stage 3 (MIS 3 27–60 ka). At this time, dust flux to Antarctica was low, and therefore, iron fertilization was restricted, but sea-ice was expanded relative to today and as extensive as during the LGM [*Wolff et al.,* 2006]. In a previous modeling study [*Matsumoto et al.,* 2014], we found that when sea-ice extent is increased 50% relative to today, in the presence of modern-like Fe inputs, some leakage of Si from the Southern Ocean does occur, as manifested by higher Si concentrations in intermediate waters leaving the Southern Ocean. However, the impact on floral composition, opal flux, and $CaCO_3$:organic C rain rate outside the Southern Ocean is modest. In the model, a dipole response to sea-ice expansion is observed, where opal flux in the southern part of the Southern Ocean decreases strongly with sea-ice expansion while opal flux in the northern part of the Southern Ocean increases with increased sea-ice. In the model at least, most of the extra silicic acid exported from the Antarctic region in response to sea-ice expansion is consumed in the sub-Antarctic and therefore not available to be exported to low latitudes, a result that depends on low iron availability to stimulate Si consumption in the sub-Antarctic. However, limited proxy records from the sub-Antarctic across MIS 3 show opal flux generally tracks terrigenous deposition in marine sediments and dust deposition in Antarctic ice cores [*Anderson et al.,* 2014; *Kienast et al.,* 2006], suggesting iron addition stimulates annual opal flux in this region, at least during MIS 3. Indeed, a Si isotope record from the Pacific sub-Antarctic (NBP9802-9PC2) shows remarkable coherence with the Antarctic ice core dust deposition record [*Robinson et al.,* 2014], suggesting Si

consumption increases with increasing iron availability. Although changes in the upwelling supply of Si may also be involved in explaining the MIS 3 opal flux behavior [*Hayes et al.,* 2011; *Anderson et al.,* 2014], these observations support the possibility that during periods of coincident sea-ice expansion and low iron flux, Si exported from the Antarctic zone is not consumed in the sub-Antarctic and may indeed reach equatorial latitudes [*Kienast et al.,* 2006].

Proxy records from the sub-Antarctic (where we know sea-ice is not a factor) also support a positive relationship between dust flux and opal production on glacial-interglacial timescales. This relationship is seen both temporally at a single site, where opal flux tracks terrigenous flux [e.g., *Frank et al.,* 2000], and in considering the spatial distribution across the sub-Antarctic, where opal flux in the Pacific sector during the LGM is lower than in the Atlantic and Indian sectors, consistent with dust input to the Pacific being the lowest [*Chase et al.,* 2003; *Bradtmiller et al.,* 2009; *Lamy et al.,* 2014].

The above discussion suggests that the Southern Ocean operated differently during glacial climates (iron flux and opal production are positively related) compared to today, when purposeful and natural iron fertilization experiments indicate an inverse relationship for iron supply and opal production. In MESMO2, the negative influence of iron on silicification outweighs the positive influence on diatom growth rate, such that opal production generally decreases with iron addition, consistent with the modern observations. In contrast, in the PISCES model [*Tagliabue et al.,* 2014] the effect of iron on diatom growth outweighs the effect on diatom stoichiometry, such that a decrease in iron supply leads to a decrease in opal flux, consistent with the glacial climate observations. It is important to keep in mind, however, that these models did not use identical boundary conditions. For example, experiment ALL with MESMO2 [*Matsumoto et al.,* 2014] used an idealized and convenient set of glacial boundary conditions. Depending on the relative strength of these boundary conditions, some of which cancel one another (e.g., greater ice and larger iron input would have opposing effects on opal production), the net effect on opal export could be quite different. More work is needed to better understand the controls on Si utilization and export in the Southern Ocean, and on the role of iron in particular.

5. Summary and Conclusions

In this paper we present an expanded compilation of Th-normalized opal burial rates at 188 sites and opal concentration measurements from 496 sites in the Southern Ocean, to estimate overall opal burial rates and to use these more extensive data to better understand controls on opal rain rates. Using a bioregionalization approach we estimate biogenic Si burial in the Southern Ocean at $2.3 +/- 1.0$ Tmol Si yr^{-1}, a number consistent with recent estimates. Similar to previous studies, highest burial is found in the opal belt, bound to the north by low silicic acid availability and to the south by the length of the ice-free growing season. Our bioregionalization approach also reveals several regions where data are scant, notably the Antarctic shelves and the northern temperate regions of the Southern Ocean.

We compared opal burial rates with seven environmental parameters and found that the factors controlling opal burial rates were different in predominantly ice-covered and ice-free regions. In ice-covered regions, the dominant variables included number of ice-covered days, winter mixed layer depth, and preservation efficiency. In ice-free areas, the dominant explanatory variables were autumn surface water silicic acid concentration and sea surface temperature, with autumn mixed layer depth, total Th-normalized flux, and dust flux contributing additional explanatory power to the relationship. Opal burial is not correlated with dust flux alone, a result that may reflect the decoupling between carbon and opal under the influence of iron: low iron conditions promote a small production of heavily silicified diatoms, whereas higher iron levels promote a larger production of weakly silicified diatoms, the net result being that iron is not a good predictor of total opal rain to the seafloor.

We corrected opal burial rates for postdepositional opal dissolution using the algorithm of *Sayles et al.* [2001], which predicts opal preservation from total sediment flux. We find good agreement between the observed corrected opal rain to the seafloor and those predicted from MESMO2, an earth system model of intermediate complexity [*Matsumoto et al.,* 2013], both in magnitude and geographic distribution. However, the observed corrected opal rain rates tend to be smaller than the model predictions in the north and larger in the south. One explanation for this mismatch is that it reflects the need for a better preservation algorithm, in particular one that incorporates sediment components such as Al:Si ratio.

Given that opal fluxes have been used as indicators of changes in sea-ice, export production, stratification, and upwelling intensity, this work has several interesting implications for the interpretation of opal burial as a paleo-proxy:

1. The duration of sea-ice cover places a maximum limit on the opal burial that is likely to be observed, but several additional factors can reduce opal burial rates so that the reverse interpretation is difficult (i.e., decreased opal burial rates alone are not an indicator of increased sea-ice). At the same time, there may be potential to improve reconstructions of summer and winter sea-ice extent by including opal burial rates with diatom-assemblage information.
2. This work demonstrates that in ice-free regions, opal burial is related to changes in surface water silicic acid concentrations. Insofar as silicic acid supply can be linked to changes in upwelling and stratification, this analysis could support changes in opal burial as representative of changes in upwelling/stratification in the sediment record [e.g., *Anderson et al.,* 2009]. However, although factors associated with silicic acid availability (temperature and MLD) are statistically significant predictors of opal flux in the ice-free regions today (see above), their predictive power is modest and indirectly linked to upwelling. Furthermore, during glacial times, regions that are today ice free may have been seasonally ice covered. As we have shown that even small changes in sea-ice duration during the year can have a large impact on opal burial, the role of changes in sea-ice duration needs to be carefully considered in interpretations of opal flux records south of the APF.
3. In terms of export production, this study emphasizes the decoupling between opal and carbon export in the Southern Ocean. Opal burial rates are not linked strongly with satellite-based estimates of net primary production or iron concentrations (represented as simulated dust flux).

Overall, this work supports the view that patterns of sedimentary opal burial in the Southern Ocean are controlled primarily by the surface ocean factors that control biogenic silica production and export. Ongoing work to understand the processes controlling opal production and export will aid interpretation of the sedimentary record. Although factors affecting opal preservation on the seafloor are of secondary importance, additional work to understand these factors is also needed to fully exploit the sedimentary record of opal burial.

Acknowledgments

The compilation of Th-normalized opal burial rates and opal concentration is available from PANGEA (http://issues.pangaea.de/browse/PDI-9945). Data on environmental climatologies are available as detailed in Table 2 and from Z.C. (zchase@utas.edu.au). MESMO2 model output is available from K.M. (katsumi@umn.edu). Travel funding was provided to K.E.K. and K.M. by the University of Tasmania Visiting Scholar Program. Z.C. is supported by an Australian Research Council Future Fellowship. We thank B. Reutsch for her contributions at an early stage of this project. R. Massom provided for assistance with sea-ice data sets, P. Strutton helped with productivity data sets and pointed us to the Bioregionalization, and S. Wotherspoon provided statistical advice. Numerical computation involving MESMO was carried out using resources at the University of Minnesota Supercomputing Institute. Finally, we would like to sincerely acknowledge Lloyd Burckle, for his passion for and vast knowledge of Southern Ocean opal dynamics and for sharing with us his Southern Ocean sediment composition database.

References

Abelmann, A., R. Gersonde, G. Cortese, G. Kuhn, and V. Smetacek (2006), Extensive phytoplankton blooms in the Atlantic sector of the glacial Southern Ocean, *Paleoceanography*, *21*, PA1013, doi:10.1029/2005PA001199.

Anderson, R. F., N. Kumar, R. A. Mortlock, P. N. Froelich, P. Kubik, B. Dittrich-Hannen, and M. Suter (1998), Late-Quaternary changes in productivity of the Southern Ocean, *J. Mar. Syst.*, *17*, 497–514.

Anderson, R. F., S. Ali, L. I. Bradtmiller, S. Nielsen, M. Q. Fleisher, B. E. Anderson, and L. H. Burckle (2009), Wind-driven upwelling in the Southern Ocean and the deglacial rise in atmospheric CO_2, *Science*, *323*, 1443–1448.

Anderson, R. F., S. Barker, M. Fleisher, R. Gersonde, S. L. Goldstein, G. Kuhn, P. G. Mortyn, K. Pahnke, and J. P. Sachs (2014), Biological response to millennial variability of dust and nutrient supply in the Subantarctic South Atlantic Ocean, *Philos. Trans. R. Soc. A*, *372*, 20130054, doi:10.1098/rsta.2013.0054.

Archer, D., A. Winguth, D. Lea, and N. Mahowald (2000), What caused the glacial/interglacial atmospheric pCO_2 cycles?, *Rev. Geophys.*, *38*, 159–189, doi:10.1029/1999RG000066.

Armand, L. K., V. Cornet-Barthaux, J. Mosseri, and B. Quéguiner (2008), Late summer diatom biomass and community structure on and around the naturally iron-fertilised Kerguelen Plateau in the Southern Ocean, *Deep Sea Res., Part II*, *55*, 653–676.

Arrigo, K. R. (2014), Sea ice ecosystems, *Annu. Rev. Mar. Sci.*, *6*, 439–467, doi:10.1146/annurev-marine-010213-135103.

Assmy, P., V. Smetacek, M. Montresor, C. Klaas, J. Henjes, V. H. Strass, J. M. Arrieta, U. Bathmann, G. M. Berg, and E. Breitbarth (2013), Thick-shelled, grazer-protected diatoms decouple ocean carbon and silicon cycles in the iron-limited Antarctic Circumpolar Current, *Proc. Natl. Acad. Sci. U.S.A.*, *110*, 20,633–20,638.

Blain, S., et al. (2007), Effect of natural iron fertilization on carbon sequestration in the Southern Ocean, *Nature*, *446*, 1070–1074, doi:10.1038/nature05700.

Boyd, P. W., et al. (2000), A mesoscale phytoplankton bloom in the polar Southern Ocean stimulated by iron fertilization, *Nature*, *407*, 695–702.

Boyd, P. W., D. S. Mackie, and K. A. Hunter (2010), Aerosol iron deposition to the surface ocean—Modes of iron supply and biological responses, *Mar. Chem.*, *120*, 128–143, doi:10.1016/j.marchem.2009.01.008.

Bradtmiller, L. I., R. F. Anderson, M. Q. Fleisher, and L. H. Burckle (2009), Comparing glacial and Holocene opal fluxes in the Pacific sector of the Southern Ocean, *Paleoceanography*, *24*, PA2214, doi:10.1029/2008PA001693.

Brzezinski, M. A., C. Pride, V. M. Franck, D. Sigman, J. L. Sarmiento, K. Matsumoto, N. Gruber, G. H. Rau, and K. H. Coale (2002), A switch from $Si(OH)_4$ to NO_3^- depletion in the glacial Southern Ocean, *Geophys. Res. Lett.*, *29*(12), 1564, doi:10.1029/2001GL014349.

Burckle, L. H., and J. Cirilli (1987), Origin of diatom ooze belt in the Southern Ocean: Implications for late Quaternary paleoceanography, *Micropaleontology*, *33*, 82–86.

Cassar, N., M. L. Bender, B. A. Barnett, S. Fan, W. J. Moxim, H. Levy, and B. Tilbrook (2007), The Southern Ocean biological response to aeolian iron deposition, *Science*, *317*, 1067–1070, doi:10.1126/science.1144602.

Charles, C. D., P. N. Froelich, M. A. Zibello, R. A. Mortlock, and J. J. Morley (1991), Biogenic opal in Southern Ocean sediments over the last 450,000 years: Implications for surface water chemistry and circulation, *Paleoceanography*, *6*, 697–728, doi:10.1029/91PA02477.

Chase, Z., R. F. Anderson, M. Q. Fleisher, and P. W. Kubik (2003), Accumulation of biogenic and lithogenic material in the Pacific sector of the Southern Ocean during the past 40,000 years, *Deep Sea Res., Part II*, *50*, 799–832, doi:10.1016/S0967-0645(02)00595-7.

Coale, K. H., et al. (2004), Southern Ocean iron enrichment experiment: Carbon cycling in high- and low-Si waters, *Science*, *304*, 408–414.

Cooke, D. W., and J. D. Hays (1982), Estimates of Antarctic Ocean seasonal sea-ice cover during glacial intervals, in *Proceedings of the Third Symposium on Antarctic Geosciences*, edited by C. Craddock, pp. 1017–1025, Univ. of Wis. Press, Madison, Wis.

Crosta, X., J. J. Pichon, and L. H. Burckle (1998), Application of modern analog technique to marine Antarctic diatoms: Reconstructions of maximum sea-ice extent at the Last Glacial Maximum, *Paleoceanography*, *13*, 284–297, doi:10.1029/98PA00339.

Curran, M. A., T. D. van Ommen, V. I. Morgan, K. L. Phillips, and A. S. Palmer (2003), Ice core evidence for Antarctic sea ice decline since the 1950s, *Science*, *302*, 1203–1206.

Death, R., J. L. Wadham, F. Monteiro, A. M. Le Brocq, M. Tranter, A. Ridgwell, S. Dutkiewicz, and R. Raiswell (2014), Antarctic ice sheet fertilises the Southern Ocean, *Biogeosciences*, *11*, 2635–2643, doi:10.5194/bg-11-2635-2014-supplement.

DeMaster, D. J. (1981), The supply and accumulation of silica in the marine environment, *Geochim. Cosmochim. Acta*, *45*, 1715–1732.

DeMaster, D. J. (2002), The accumulation and cycling of biogenic silica in the Southern Ocean: Revisiting the marine silica budget, *Deep Sea Res., Part II*, *49*, 3155–3167.

DeMaster, D. J., O. Ragueneau, and C. A. Nittrouer (1996), Preservation efficiencies and accumulation rates for biogenic silica and organic C, N, and P in high-latitude sediments: The Ross Sea, *J. Geophys. Res.*, *101*, 18,501–18,518, doi:10.1029/96JC01634.

Dezileau, L., G. Bareille, J. L. Reyss, and F. Lemoine (2000), Evidence for strong sediment redistribution by bottom currents along the southeast Indian ridge, *Deep Sea Res., Part I*, *47*, 1899–1936.

Dezileau, L., J. L. Reyss, and F. Lemoine (2003), Late Quaternary changes in biogenic opal fluxes in the Southern Indian Ocean, *Mar. Geol.*, *202*, 143–158, doi:10.1016/S0025-3227(03)00283-4.

Dixit, S., and P. Van Cappellen (2003), Predicting benthic fluxes of silicic acid from deep-sea sediments, *J. Geophys. Res.*, *108*(C10), 3334, doi:10.1029/2002JC001309

Dixit, S., P. Van Cappellen, and A. J. Van Bennekom (2001), Processes controlling solubility of biogenic silica and pore water build-up of silicic acid in marine sediments, *Mar. Chem.*, *73*, 333–352.

Fennel, K., M. R. Abbott, Y. H. Spitz, J. G. Richman, and D. M. Nelson (2003), Impacts of iron control on phytoplankton production in the modern and glacial Southern Ocean, *Deep Sea Res., Part II*, *50*, 833–851.

Francois, R., M. Frank, M. M. Rutgers van der Loeff, and M. P. Bacon (2004), ^{230}Th normalization: An essential tool for interpreting sedimentary fluxes during the late Quaternary, *Paleoceanography*, *19*, PA1018, doi:10.1029/2003PA000939.

Frank, M., R. Gersonde, and A. Mangini (1999), Sediment redistribution, ^{230}Thex-normalization and implications for the reconstruction of particle flux and export paleoproductivity, in *Use of Proxies in Paleoceanography*, edited by G. G. Fischer and G. Wefer, pp. 409–426, Springer, Berlin.

Frank, M., R. Gersonde, M. M. Rutgers van der Loeff, G. Bohrmann, C. C. Nurnberg, P. W. Kubik, M. Suter, and A. Mangini (2000), Similar glacial and interglacial export bioproductivity in the Atlantic sector of the Southern Ocean: Multiproxy evidence and implications for glacial atmospheric CO_2, *Paleoceanography*, *15*, 642–658, doi:10.1029/2000PA000497.

Geibert, W., M. M. R. van der Loeff, R. Usbeck, R. Gersonde, G. Kuhn, and J. Seeberg-Elverfeldt (2005), Quantifying the opal belt in the Atlantic and southeast Pacific sector of the Southern Ocean by means of Th-230 normalization, *Global Biogeochem. Cycles*, *19*, GB4001, doi:10.1029/2005GB002465.

Grant, S., A. J. Constable, B. Raymond, and S. Doust (2006), Bioregionalisation of the Southern Ocean: Report of Experts Workshop, Hobart, WWF-Australia and ACE CRC, Sept.

Hayes, C. T., R. F. Anderson, and M. Q. Fleisher (2011), Opal accumulation rates in the equatorial Pacific and mechanisms of deglaciation, *Paleoceanography*, *26*, PA1207, doi:10.1029/2010PA002008.

Honjo, S., R. Francois, S. Manganini, J. Dymond, and R. Collier (2000), Particle fluxes to the interior of the Southern Ocean in the Western Pacific sector along 170°W, *Deep Sea Res., Part II*, *47*, 3521–3548.

Jaccard, S. L., C. T. Hayes, A. Martinez-Garcia, D. A. Hodell, R. F. Anderson, D. M. Sigman, and G. H. Haug (2013), Two modes of change in Southern Ocean productivity over the past million years, *Science*, *339*, 1419–1423, doi:10.1126/science.1227545.

Johnson, R., P. G. Strutton, S. W. Wright, A. McMinn, and K. M. Meiners (2013), Three improved satellite chlorophyll algorithms for the Southern Ocean, *J. Geophys. Res. Oceans*, *118*, 3694–3703, doi:10.1002/jgrc.20270.

Kienast, S., M. Kienast, S. Jaccard, S. Calvert, and R. Francois (2006), Testing the silica leakage hypothesis with sedimentary opal records from the eastern equatorial Pacific over the last 150 kyrs, *Geophys. Res. Lett.*, *33*, L15607, doi:10.1029/2006GL026651.

Kumar, N. (1994), Trace metals and natural radionuclides as tracers of ocean productivity, PhD thesis, Columbia Univ., New York.

Lamy, F., R. Gersonde, G. Winckler, O. Esper, A. Jaeschke, G. Kuhn, J. Ullermann, A. Martinez-Garcia, F. Lambert, and R. Kilian (2014), Increased dust deposition in the Pacific Southern Ocean during glacial periods, *Science*, *343*, 403–407, doi:10.1126/science.1245424.

Le Quéré, C., L. Bopp, and I. Tegen (2002), Antarctic circumpolar wave impact on marine biology: A natural laboratory for climate change study, *Geophys. Res. Lett.*, *29*(10), 1407, doi:10.1029/2001GL014585.

Leynaert, A., D. M. Nelson, B. Queguiner, and P. Treguer (1993), The silica cycle in the Antarctic Ocean: Is the Weddell Sea atypical, *Mar. Ecol. Prog. Ser.*, *96*, 1–15.

Leynaert, A., E. Bucciarelli, P. Claquin, R. C. Dugdale, V. Martin-Jézéquel, P. Pondaven, and O. Ragueneau (2004), Effect of iron deficiency on diatom cell size and silicic acid uptake kinetics, *Limnol. Oceanogr.*, *49*, 1134–1143.

Lisitzin, A. P. (1971), Distribution of siliceous microfossils in suspension and in bottom sediments, in *The Micropaleontology of Oceans*, edited by B. M. Funnell and W. R. Reidel, pp. 173–195, Cambridge Univ. Press, Cambridge.

Mahowald, N. M., D. R. Muhs, S. Levis, P. J. Rasch, M. Yoshioka, C. S. Zender, and C. Luo (2006), Change in atmospheric mineral aerosols in response to climate: Last glacial period, preindustrial, modern, and doubled carbon dioxide climates, *J. Geophys. Res.*, *111*, D10202, doi:10.1029/2005JD006653.

Marchetti, A., and P. J. Harrison (2007), Coupled changes in the cell morphology and the elemental (C, N, and Si) composition of the pennate diatom Pseudo-nitzschia due to iron deficiency, *Limnol. Oceanogr.*, *52*, 2270–2284.

Matsumoto, K., J. L. Sarmiento, and M. A. Brzezinski (2002), Silicic acid "leakage" from the Southern Ocean: A possible explanation for glacial atmospheric pCO_2, *Global Biogeochem. Cycles*, *16*(3), 1031, doi:10.1029/2001GB001442.

Matsumoto, K., K. Tokos, A. R. Price, and S. Cox (2008), First description of the Minnesota earth system model for ocean biogeochemistry (MESMO 1.0), *Geosci. Model Dev.*, *1*, 1–15.

Matsumoto, K., K. Tokos, A. Huston, and H. Joy-Warren (2013), MESMO 2: A mechanistic marine silica cycle and coupling to a simple terrestrial scheme, *Geosci. Model Dev.*, *6*, 477–494, doi:10.5194/gmd-6-477-2013.

Matsumoto, K., Z. Chase, and K. Kohfeld (2014), Different mechanisms of silicic acid leakage and their biogeochemical consequences, *Paleoceanography*, *29*, 238–254, doi:10.1002/2013PA002588.

Moore, J. K., and M. R. Abbott (2000), Phytoplankton chlorophyll distributions and primary production in the Southern Ocean, *J. Geophys. Res.*, *105*, 28,709–28,722, doi:10.1029/1999JC000043.
Mortlock, R. A., and P. N. Froelich (1989), A simple method for the rapid determination of biogenic opal in pelagic marine sediments, *Deep Sea Res., Part I*, *36*, 1415–1426.
Mortlock, R. A., C. D. Charles, P. N. Froelich, M. A. Zibello, J. Saltzman, J. D. Hays, and L. H. Burckle (1991), Evidence for lower productivity in the Antarctic Ocean during the last glaciation, *Nature*, *351*, 220–223.
Mosseri, J., B. Queguiner, L. Armand, and V. Cornet-Barthaux (2008), Impact of iron on silicon utilization by diatoms in the Southern Ocean: A case study of Si/N cycle decoupling in a naturally iron-enriched area, *Deep Sea Res., Part II*, *55*, 801–819, doi:10.1016/j.dsr2.2007.12.003.
Nelson, D. M., et al. (2002), Vertical budgets for organic carbon and biogenic silica in the Pacific Sector of the Southern Ocean, 1996–1998, *Deep Sea Res., Part II*, *49*, 1645–1673.
Nodder, S. D., P. W. Boyd, S. M. Chiswell, M. H. Pinkerton, J. M. Bradford-Grieve, and M. J. N. Greig (2005), Temporal coupling between surface and deep ocean biogeochemical processes in contrasting subtropical and subantarctic water masses, southwest Pacific Ocean, *J. Geophys. Res.*, *110*, C12017, doi:10.1029/2004JC002833.
Orsi, A. H., T. Whitworth, and N. Worth (1995), On the meridional extent and fronts of the Antarctic Circumpolar Current, *Deep Sea Res., Part I*, *42*, 641–673.
Parkinson, C. L. (1994), Spatial patterns in the length of the sea ice season in the Southern Ocean, 1979–1986, *J. Geophys. Res.*, *99*, 16,327–16,339, doi:10.1029/94JC01146.
Pichevin, L. E., B. C. Reynolds, R. S. Ganeshram, I. Cacho, L. Pena, K. Keefe, and R. M. Ellam (2009), Enhanced carbon pump inferred from relaxation of nutrient limitation in the glacial ocean, *Nature*, *459*, 1114–1117, doi:10.1038/nature08101.
Pollard, R. T., et al. (2009), Southern Ocean deep-water carbon export enhanced by natural iron fertilization, *Nature*, *457*, 577–580, doi:10.1038/nature07716.
Pondaven, P., O. Ragueneau, P. Treguer, A. Hauvespre, L. Dezileau, and J. L. Reyss (2000), Resolving the "opal paradox" in the Southern Ocean, *Nature*, *405*, 168–172.
Ragueneau, O., et al. (2001), The benthic silica cycle in the Northeast Atlantic: Annual mass balance, seasonality, and importance of non-steady-state processes for the early diagenesis of biogenic opal in deep-sea sediments, *Prog. Oceanogr.*, *50*, 171–200.
Ragueneau, O., N. Dittert, P. Pondaven, and P. Treguer (2002), Si/C decoupling in the world ocean: Is the Southern Ocean different?, *Deep Sea Res., Part II*, *49*, 3127–3154.
Reynolds, R. W., N. A. Rayner, T. M. Smith, D. L. Stokes, and W. Wang (2002), An improved in situ and satellite SST analysis for climate, *J. Clim.*, *15*, 1609–1625.
Robinson, R. S., M. A. Brzezinski, C. P. Beucher, M. G. S. Horn, and P. Bedsole (2014), The changing roles of iron and vertical mixing in regulating nitrogen and silicon cycling in the Southern Ocean over the last glacial cycle, *Paleoceanography*, *29*, 1179–1195, doi:10.1002/2014PA002686.
Rysgaard, S., T. G. Nielsen, and B. W. Hansen (1999), Seasonal variation in nutrients, pelagic primary production and grazing in a high-Arctic coastal marine ecosystem, Young Sound, Northeast Greenland, *Mar. Ecol. Prog. Ser.*, *179*, 13–25.
Salter, I., R. S. Lampitt, R. Sanders, A. Poulton, A. E. S. Kemp, B. Boorman, K. Saw, and R. Pearce (2007), Estimating carbon, silica and diatom export from a naturally fertilised phytoplankton bloom in the Southern Ocean using PELAGRA: A novel drifting sediment trap, *Deep Sea Res., Part II*, *54*, 2233–2259, doi:10.1016/j.dsr2.2007.06.008.
Sarmiento, J. L., and N. Gruber (2006), *Ocean Biogeochemical Dynamics*, Princeton Univ. Press, Princeton, N. J.
Sarmiento, J. L., N. Gruber, M. A. Brzezinski, and J. P. Dunne (2004), High-latitude controls of thermocline nutrients and low latitude biological productivity, *Nature*, *427*, 56–60, doi:10.1038/nature02127.
Sayles, F. L., W. R. Martin, Z. Chase, and R. F. Anderson (2001), Benthic remineralization and burial of biogenic SiO_2, $CaCO_3$, organic carbon, and detrital material in the Southern Ocean along a transect at 170 West, *Deep Sea Res., Part II*, *48*, 4323–4383.
Serno, S., G. Winckler, R. F. Anderson, C. T. Hayes, H. Ren, R. Gersonde, and G. H. Haug (2014), Using the natural spatial pattern of marine productivity in the Subarctic North Pacific to evaluate paleoproductivity proxies, *Paleoceanography*, *29*, 438–453, doi:10.1002/2013PA002594.
Sigman, D. M., S. L. Jaccard, and G. H. Haug (2004), Polar ocean stratification in a cold climate, *Nature*, *428*, 59–63, doi:10.1038/nature02357.
Sigmon, D. E., D. M. Nelson, and M. A. Brzezinski (2002), The Si cycle in the Pacific sector of the Southern Ocean: Seasonal diatom production in the surface layer and export to the deep sea, *Deep Sea Res., Part II*, *49*, 1747–1763.
Smetacek, V., et al. (2012), Deep carbon export from a Southern Ocean iron-fertilized diatom bloom, *Nature*, *487*, 313–319, doi:10.1038/nature11229.
Sokolov, S., and S. R. Rintoul (2009), Circumpolar structure and distribution of the Antarctic Circumpolar Current fronts: 1. Mean circumpolar paths, *J. Geophys. Res.*, *114*, C11018, doi:10.1029/2008JC005108.
Stammerjohn, S. E., D. G. Martinson, R. C. Smith, X. Yuan, and D. Rind (2008), Trends in Antarctic annual sea ice retreat and advance and their relation to El Niño–Southern Oscillation and Southern Annular Mode variability, *J. Geophys. Res.*, *113*, C03S90, doi:10.1029/2007JC004269.
Stroeve, J. (2003), Sea Ice Trends and Climatologies from SMMR and SSM/I-SSMIS, Version 1. [1979–2006], NASA National Snow and Ice Data Center Distributed Active Archive Center, Boulder, Colo. doi:10.5067/C2HMG48G83QQ.
Tagliabue, A., O. Aumont, and L. Bopp (2014), The impact of different external sources of iron on the global carbon cycle, *Geophys. Res. Lett.*, *41*, 920–926, doi:10.1002/2013GL059059.
Takeda, S. (1998), Influence of iron availability on nutrient consumption ratio of diatoms in oceanic waters, *Nature*, *393*, 774–777.
Treguer, P., and A. J. Van Bennekom (1991), The annual production of biogenic silica in the Antarctic Ocean, *Mar. Chem.*, *35*, 477–487, doi:10.1016/S0304-4203(09)90038-X.
Tréguer, P. J. (2014), The Southern Ocean silica cycle, *C. R. Geosci.*, *346*, 279–286, doi:10.1016/j.crte.2014.07.003.
Tréguer, P. J., and C. L. De La Rocha (2013), The world ocean silica cycle, *Annu. Rev. Mar. Sci.*, *5*, 477–501, doi:10.1146/annurev-marine-121211-172346.
Trull, T. W., S. R. Rintoul, M. Hadfield, and E. R. Abraham (2001a), Circulation and seasonal evolution of polar waters south of Australia: Implications for iron fertilization of the Southern Ocean, *Deep Sea Res., Part II*, *48*, 2439–2466.
Trull, T. W., S. G. Bray, S. J. Manganini, S. Honjo, and R. Francois (2001b), Moored sediment trap measurements of carbon export in the Subantarctic and Polar Frontal Zones of the Southern Ocean, south of Australia, *J. Geophys. Res.*, *106*, 31,489–31,509, doi:10.1029/2000JC000308.
Van Cappellen, P., and L. Qiu (1997), Biogenic silica dissolution in sediments of the Southern Ocean. I. Solubility, *Deep Sea Res., Part II*, *44*, 1109–1128.
Warnock, J., R. Scherer, and P. Loubere (2007), A quantitative assessment of diatom dissolution and late quaternary primary productivity in the eastern equatorial Pacific, *Deep Sea Res., Part II*, *54*, 772–783.

Westberry, T., M. J. Behrenfeld, D. A. Siegel, and E. Boss (2008), Carbon-based primary productivity modeling with vertically resolved photoacclimation, *Global Biogeochem. Cycles*, *22*, GB2024, doi:10.1029/2007GB003078.

Wolff, E. W., et al. (2006), Southern Ocean sea-ice extent, productivity and iron flux over the past eight glacial cycles, *Nature*, *440*, 491–496, doi:10.1038/nature04614.

Yu, E.-F. (1994), Variations in the particulate flux of 230Th and 231 Pa and paleoceanographic applications of the 231 Pa/230Th ratio, PhD thesis, Woods Hole Oceanogr. Inst., and Mass. Inst. of Technol.